

The Use of Simultaneous Horizontal and Vertical Transmissions for Dual-Polarization Radar Meteorological Observations

RICHARD D. SCOTT,* PAUL R. KREHBIEL, AND WILLIAM RISON

*Langmuir Laboratory for Atmospheric Research, Geophysical Research Center,
New Mexico Institute of Mining and Technology, Socorro, New Mexico*

(Manuscript received 17 May 1999, in final form 31 July 2000)

ABSTRACT

Observations are presented in which the standard dual-polarization meteorological quantities (Z_{DR} , ϕ_{dp} , and ρ_{HV}) are determined from simultaneous horizontal (H) and vertical (V) transmissions. The return signals are measured in parallel H and V receiving channels. Because the parameters are determined from simultaneous measurements they are not affected by Doppler phase shifts that increase the variance of ϕ_{dp} and ρ_{HV} when alternating H and V polarizations are transmitted. The approach has the additional advantage that a high-power polarization switch is not needed. The relative phases of the H and V components were such that the transmitted polarization was circular. Circular polarization is shown to detect horizontally oriented particles such as rain with the same effectiveness as linearly polarized transmissions, and optimally detects randomly oriented or shaped particles such as hail. Circular polarization also optimally senses nonhorizontally oriented particles such as electrically aligned ice crystals. By not needing to alternate between H and V transmissions it becomes practical to make polarization-diverse measurements by transmitting other orthogonal polarizations on successive pulses (e.g., left-hand circular and $+45^\circ$ slant linear) to aid in identifying precipitation types. It is shown that ρ_{HV} from simultaneous transmissions provides the same information on randomly oriented scatterers as the linear depolarization ratio LDR from H or V transmissions, and that LDR does not need to be measured when information on particle canting is not important or is not needed.

1. Introduction

Most dual-polarization meteorological radars transmit and receive in the same polarization basis. For example, radars that operate in an H - V basis typically transmit alternate pulses of horizontal (H) and vertical (V) polarized radiation and receive the backscattered returns in the same polarization as transmitted (the copolar return), and sometimes in the orthogonal polarization (the cross-polar return). Radars that operate in a circular polarization basis transmit a given circular polarization [left-hand circular (LHC) or right-hand circular (RHC)] and receive the backscattered signals in parallel LHC and RHC channels to obtain the dual-polarization measurements. Alternate pulses of LHC and RHC radiation can also be transmitted. For a summary of the characteristics of a number of polarization diversity radars, see Bringi and Hendry (1990).

In this paper we describe results from a hybrid approach in which H and V signals are transmitted simultaneously, in this case in the form of circular polarization, and are received in parallel H and V channels. The transmitted and received signals are in different polarization bases, so that the received signals are both copolar-like.

Because raindrops are horizontally flattened by aerodynamic forces as they fall, measurements in an H - V basis provide important information on liquid precipitation. Of particular interest in this regard is the differential reflectivity $Z_{DR} = Z_H/Z_V$ for H and V transmissions (e.g., Seliga and Bringi 1976; Hall et al. 1980, 1984) and the differential phase ϕ_{HV} of H and V returns, which changes progressively with range in propagating through rain (e.g., McCormick and Hendry 1975; Seliga and Bringi 1978; Jameson and Mueller 1985; Sachidananda and Zrnić 1986). Also of interest is the copolar-copolar H - V correlation coefficient $\rho_{HV}(0)$, which detects shape variation in horizontally oriented particles (e.g., Jameson 1983, 1985; Sachidananda and Zrnić 1985), and irregularly shaped particles such as hail (e.g., Balakrishnan and Zrnić 1990).

Each of the above quantities needs to be measured at "zero lag," namely, as if the H and V polarizations were transmitted simultaneously. Instead of actually using si-

* Current affiliation: Teledyne Electronic Technologies, Mountain View, California.

Corresponding author address: Dr. Paul R. Krehbiel, Langmuir Laboratory for Atmospheric Research, New Mexico Institute of Mining and Technology, Socorro, NM 87801.
E-mail: krehbiel@ibis.nmt.edu.

multaneous transmissions, the measurements have traditionally been obtained by transmitting alternate H and V polarizations and receiving the backscattered returns in the same polarization as transmitted. The differential reflectivity Z_{DR} is determined from the ratio of the copolar backscattered powers, and ϕ_{HV} is determined by coherently correlating the H and V returns from successive pairs of transmitted pulses. The phase differences of the H and V returns are substantially affected by the pulse-to-pulse Doppler shift, which needs to be separated out from the desired propagation phase shift. The Doppler contribution is canceled out by correlating interlaced sets of pulse pairs, $R_a = \langle H^*V \rangle$ and $R_b = \langle V^*H \rangle$, and by differencing the arguments of the two quantities (Mueller 1984). The random nature of the Doppler phase shift from one pulse to the next increases the uncertainty of the ϕ_{HV} estimate (Sachidananda and Zrnić 1986), adding noise to an already weak effect. Similar difficulties beset the ρ_{HV} measurements. The normalized magnitudes of R_a and R_b give $\rho_{HV}(T)$, where T is the interpulse interval. The correlation coefficient $\rho_{HV}(T)$ is reduced from the correlation $\rho_{HV}(0)$ at zero time lag by the Doppler effects, which decorrelate the signal during the interpulse interval. The zero-lag value can be estimated from $\rho_{HV}(T)$ by assuming a Gaussian Doppler spectrum (Balakrishnan and Zrnić 1990), but the uncertainty of the estimate is increased both by the random nature of the Doppler signal and possibly by the Gaussian spectral assumption. The estimator algorithms and variances are well summarized by Doviak and Zrnić (1993).

The alternate H - V transmission technique has been utilized because it requires only a single receiving channel, which tends to be well matched with itself. Also, by using a second receiver channel to measure the cross-polar return, one can determine the linear depolarization ratio LDR. In addition to the measurements being affected by the interpulse Doppler shift, a high-power polarization switch is needed to alternate between the H and V transmissions.

The advantage of transmitting and receiving H and V polarizations simultaneously is that ϕ_{HV} , ρ_{HV} , and Z_{DR} are determined directly from the same transmitted pulse, that is, at zero lag, and are not contaminated by Doppler effects. Also, a polarization switch is not needed. Dual receiving channels are required, but modern receiving techniques enable these to be implemented in a highly matched manner. Dwell time is reduced because the estimates can be obtained from individual transmitted pulses rather than from successive pulses, and because less averaging is needed in the absence of the Doppler effects. Alternatively, one can obtain true polarization-diverse measurements by switching between other sets of orthogonal polarizations (e.g., circular and slant 45° linear).

The simultaneous transmission approach was first suggested by Seliga and Bringi (1976) as one way of measuring Z_{DR} . It was also investigated by Sachidan-

anda and Zrnić (1985) as a way of making fast-scan differential reflectivity measurements. Both sets of investigators recognized that the approach would eliminate the effects of interpulse variations on Z_{DR} . Of equal or greater value are improved measurements of the coherent quantities ϕ_{HV} and ρ_{HV} . Jameson and Davé (1988) described how measurements in a circular polarization basis could be used to obtain the linear polarization quantities and noted that, ironically, ϕ_{HV} and ρ_{HV} would be better determined from circular polarization than from alternating linear transmissions (see also Kostinski 1994; Schultz and Kostinski 1997). Similarly, Balakrishnan and Zrnić (1990) recognized that circular polarization would be better for determining ρ_{HV} in estimating rainfall rates. In recent years the CSU-CHILL radar has been modified to transmit H and V polarizations simultaneously (as well as individually) by operating two transmitters and receivers in parallel. This eliminated the need for a polarization switch and allowed results from the alternating and simultaneous approaches to be compared (Brunkow et al. 1997, 2000; Holt et al. 1999).¹

The results reported in this paper are from the 3-cm New Mexico Tech dual-polarization radar, which utilized a power divider and an H - V polarization transducer to obtain the simultaneous transmissions. The relative phase of the two components was adjusted to produce circularly polarized radiation. In simultaneous transmission mode, the CSU-CHILL radar has typically transmitted slant 45° linear polarization. Circular and slant linear transmissions differ only in their relative phase; we later discuss the relative advantages of the two polarizations.

2. Theoretical formulations

A dual-polarization radar measures the complex amplitudes of the backscattered electric field in two orthogonal polarizations and estimates the covariances

$$\begin{aligned} W_1 &= \langle \hat{E}_1 \hat{E}_1^* \rangle, & W_2 &= \langle \hat{E}_2 \hat{E}_2^* \rangle, \\ W &= \langle \hat{E}_1 \hat{E}_2^* \rangle = |W| e^{j\phi}. \end{aligned} \quad (1)$$

Here, E_1 and E_2 denote the orthogonal components of the electric field vector and ϕ is the phase difference between the components. The polarization state of any electromagnetic wave is characterized by four quantities, in this case W_1 , W_2 , $|W|$, and $\phi = \angle W$. An alternative way of representing the covariances is in terms of the polarization ratio W_1/W_2 and the normalized cross-covariance $W/(W_1 W_2)^{1/2}$. The magnitude of the lat-

¹ A recent study by Doviak et al. (2000), published while the present paper was in its final review stages, has similarly recognized the advantages of simultaneous transmissions and recommended their use for polarimetric upgrades of the NEXRAD weather radars.

ter is the correlation coefficient of the orthogonal signals,

$$\rho = \frac{|W|}{\sqrt{W_1 W_2}}. \quad (2)$$

The three primary choices of polarization basis are (a) horizontal and vertical linear polarizations (H , V), (b) left- and right-hand circular (L , R), and (c) $\pm 45^\circ$ or slant linear polarization ($+$, $-$). When the receivers operate in an H - V basis, $W_1 = W_H$, $W_2 = W_V$, and $\rho = \rho_{HV}$. The polarization state can therefore be characterized by the quantities W_V (or W_H), W_H/W_V , ρ_{HV} , and ϕ_{HV} . We refer to these as the rationalized covariances.

The reason that an H - V basis is useful in meteorological applications is that horizontally oriented particles, in particular liquid drops, transform the rationalized covariances in a simple way. In particular, backscatter from horizontally aligned particles changes the covariances from the values incident upon a scattering volume to (Scott 1999)

$$\begin{aligned} W_V|^s &= Z_V W_V|^i, & \frac{W_H}{W_V}|^s &= Z_{DR} \frac{W_H}{W_V}|^i, \\ \rho_{HV}|^s &= f \rho_{HV}|^i, & \phi_{HV}|^s &= \delta_\ell + \phi_{HV}|^i. \end{aligned} \quad (3)$$

Here, the superscripts i and s denote the incident and scattered values, respectively. The backscattering is characterized by the reflectivity factors Z_H or Z_V ,

$$Z_H = N \langle |S_{hh}|^2 \rangle, \quad Z_V = N \langle |S_{vv}|^2 \rangle \quad (4)$$

(where N is the particle number density and $\langle |S_{hh}|^2 \rangle$, $\langle |S_{vv}|^2 \rangle$ are the reflectivity-weighted average scattering cross sections of the particles), the differential reflectivity

$$Z_{DR} = \frac{Z_H}{Z_V}, \quad (5)$$

the differential phase upon backscatter

$$\delta_\ell = \angle \langle S_{hh} S_{vv}^* \rangle, \quad (6)$$

and the parameter

$$f = \frac{|\langle S_{hh} S_{vv}^* \rangle|}{\sqrt{\langle |S_{hh}|^2 \rangle \langle |S_{vv}|^2 \rangle}} \leq 1. \quad (7)$$

The latter quantity measures the extent to which S_{hh} and S_{vv} are correlated with each other. It is usually referred to as ρ_{HV} , but this implicitly assumes that $\rho_{HV}|^i$ is unity. We denote the quantity by f to identify it as a parameter of the scatterers, as distinguished from the radar measurable ρ_{HV} . When all the particles have the same relative shape, f is unity, and when the particles have a variety of shapes f is less than unity (Jameson 1983, 1985; Balakrishnan and Zrnić 1990). The quantity f was calculated to have a value of 0.98 in rain having equilibrium drop shapes (Sachidananda and Zrnić 1985); additional calculations and experimental observations

by Illingworth and Caylor (1991) gave values between 0.985 and 0.997 in light rain.

In propagating from the radar to the scattering volume and back, the signal undergoes additional depolarization due to the effects of the propagation medium. If the medium also consists of horizontally aligned particles, several effects can occur that alter the polarization state. Differential attenuation causes the polarization ratio W_H/W_V to be reduced by attenuating the H component relative to the V component. This causes W_H/W_V incident upon the scatterers to be different from the transmitted value, according to

$$\frac{W_H}{W_V}|^i = \frac{1}{\text{DA}} \frac{W_H}{W_V}|^t. \quad (8)$$

Here, DA is the differential attenuation, defined as $\text{DA} = A_V/A_H \geq 1$, where A_V and A_H are the attenuation factors for vertical and horizontal signals, respectively. An equal amount of differential attenuation occurs in propagating back to the radar,

$$\frac{W_H}{W_V}|^r = \frac{1}{\text{DA}} \frac{W_H}{W_V}|^s. \quad (9)$$

In these expressions, the superscripts t and r denote the transmitted and received quantities, respectively. The net effect is that

$$\frac{W_H}{W_V}|^r = \frac{Z_{DR}}{(\text{DA})^2} \frac{W_H}{W_V}|^t. \quad (10)$$

Similarly, forward scattering from the aligned particles retards the phase of the horizontal component relative to the vertical, thereby reducing ϕ_{HV} . Thus,

$$\phi_{HV}|^r = -2\phi_{dp} + \delta_\ell + \phi_{HV}|^t, \quad (11)$$

where ϕ_{dp} is the one-way propagation differential phase shift. Finally, the forward scattering introduces an unpolarized component when the particles have a variety of shapes, which causes the HV correlation coefficient to be reduced. By analogy with (10),

$$\rho_{HV}|^r = f_{\text{prop}}^2 f \rho_{HV}|^t, \quad (12)$$

where f_{prop} is the one-way effect of shape variability on the propagation. The equations are completed by adding the corresponding expression for one of the reflectivity values,

$$W_V|^r = A_V^2 Z_V W_V|^t \quad \text{or} \quad (13)$$

$$W_H|^r = A_H^2 Z_H W_H|^t. \quad (14)$$

The propagation effects are cumulative with range and can significantly affect or even dominate the backscatter terms, particularly at short wavelengths. In addition, it is generally not possible to distinguish between the backscattering effect and its corresponding propagation term (e.g., Torlaschi and Holt 1993). Thus, Z_{DR} values are reduced by any cumulative differential at-

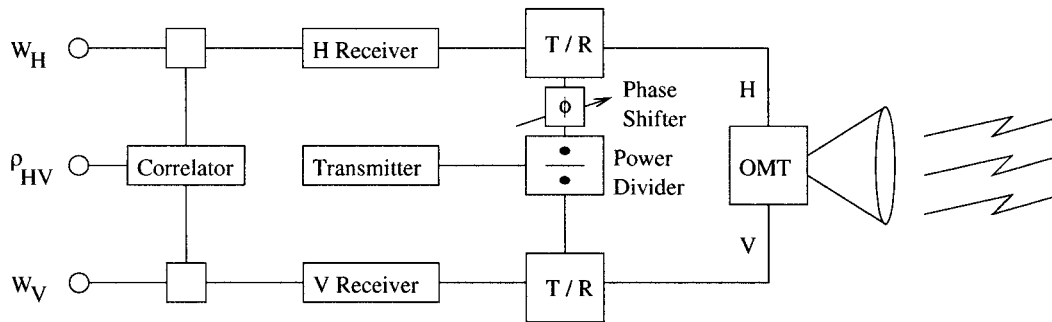


FIG. 1. Block diagram of the simultaneous transmission technique.

tenuation $(DA)^2$, and ϕ_{dp} values are affected by any differential phase upon backscatter, δ_ℓ . The presence of δ_ℓ can be identified from nonmonotonic changes in ϕ_{HV} with range (Bringi et al. 1990, 1991; Tan et al. 1991; Hubbert et al. 1993).

3. Technique and observations

The above formulations provide the basis for determining the scattering and propagation parameters from simultaneous H and V transmissions. Given the transmitted values of the covariance quantities, $W_v|'$, $(W_H/W_V)|'$, $\rho_{HV}|'$, and $\phi_{HV}|'$, the scattering and propagation parameters are determined by measuring their returned values. The transmitted values can be determined from calibration measurements and/or from the observations themselves.

Scott (1999) has analyzed the polarization changes geometrically in terms of the Poincaré sphere. One result of the analysis is that the change in the polarization state caused by Z_{DR} and by differential attenuation is greatest when the incident value of W_H/W_V is unity, namely, when the transmitted signal contains equal (or nearly equal) H and V powers. This is the situation simulated by radars that alternate between H and V transmissions, but the two polarizations can also be transmitted simultaneously. The depolarization produced by horizontally oriented particles is independent of the phase difference between the components, so that 45° linear and circular polarizations are equally effective in determining the scattering parameters. Scattering by randomly oriented particles, or by particles that are nonhorizontally aligned, is different for circular and linear polarizations, however. This can potentially be exploited to help separate out the contributions of the different particle types, as we later discuss.

Figure 1 shows the basic block diagram of the simultaneous transmission technique. A power divider replaces the polarization switch and supplies equal powers to the orthomode polarization transducer (OMT) during each transmitted pulse. By changing the relative phases of the power divider outputs the polarization can be adjusted to a variety of states ($\pm 45^\circ$ linear, LHC or RHC, or any intermediate elliptical state). For the ob-

servations reported in this paper, the polarization state was adjusted to be LHC, as viewed from the radar. The return signals are received in parallel H and V channels and processed to obtain the orthogonal powers W_H and W_V and the complex correlation coefficient $\hat{\rho}_{HV} = \rho_{HV}e^{j\phi_{HV}}$. The signals are therefore transmitted in a different polarization basis than they are received, producing a copolar-like return in each receiving channel and ensuring approximately equal signal-to-noise ratios for both signals.

The New Mexico Tech dual-polarization radar was modified during the spring of 1998 to implement the above technique. The power division was such that the transmitted H and V powers differed by 0.3 dB.² The radar transmits about 10 kW peak power at 3.0-cm wavelength and has a 3.7-m diameter Cassegrain antenna of 0.6° beamwidth. The pulse width is typically set to 1 μ s. The radar had previously been configured to transmit and receive orthogonal circular polarizations for use in studying electrically aligned ice crystals in storms (Krehiel et al. 1996). Early results of the study by Scott (1999) showed that it would be possible to measure both the electrical alignment directions and the linear polarization parameters if the circularly polarized transmissions were received in an H - V basis; this led to the simultaneous transmission approach described herein. Although arrived at in an independent manner, the technique is the same as that originally proposed by Seliga and Bringi (1976) and implemented in a slightly different manner on the CSU-CHILL radar.

a. Sample observations

Figure 2 shows observations of a relatively small but intense New Mexico storm obtained with the radar. The data are from one of a number of vigorous convective cells that occurred during passage of a frontal system through the Socorro area on 15 September (Julian day 258) 1998. The figure shows vertical cross sections of

² It is not necessary for the two powers to be exactly equal, as long as their ratio is known. The ratio is readily determined from calibration data or from the observations themselves.

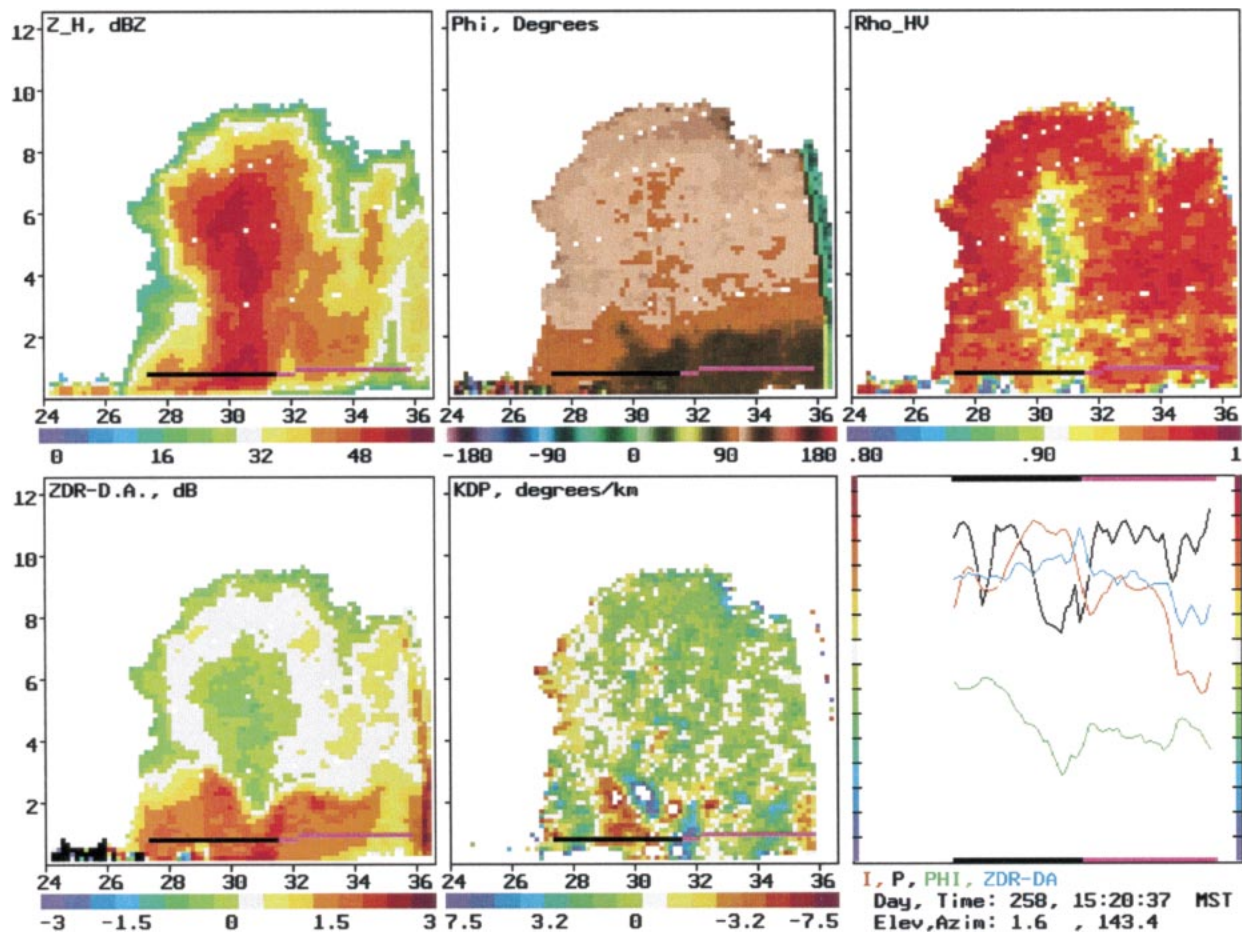


FIG. 2. Vertical cross sections of the different polarization variables through the center of a small but intense New Mexico storm, at 1520:37 MST on 15 Sep 1998. The vertical and horizontal distance scales are in km above and from the radar, respectively. The color bars show the data values in the indicated units. (lower-right) Range profiles of the different quantities along the path of the radial cursor. The vertical scale of each profile is as indicated by the vertical color bar, except for the ϕ profile, whose total vertical scale was 90° (5.6° per tick mark). In this and later figures, we have not attempted to correct reflectivity or differential reflectivity values for attenuation.

the different polarization variables through the center of the storm at the peak of the storm's vertical development. The horizontal reflectivity panel (Z_H , upper left) shows that 40 dBZ reflectivity extended up to 8-km altitude above ground level (AGL), and that detectable reflectivity extended to 10-km altitude. The radar itself was at 1.4-km altitude above mean sea level (MSL). The horizontal distance scale is in km from the radar. The red trace in the lower-right panel shows the profile of the reflectivity values along the radial cursor; the cursor is shown in black and magenta and was positioned at a low elevation angle (1.6°) to pass through the rain region of the storm.

The lower-left panel shows the pattern of differential reflectivity in the storm (as combined with differential propagation attenuation). Positive Z_{DR} (dB) values are indicated by yellow and red colors. The rain region is well delineated by the transition to positive values at and below 2- or 3-km altitude AGL. Precipitation above the transition level had neutral (i.e., nearly zero) Z_{DR}

values and was therefore frozen. The relatively strong reflectivity values in the core indicates that the precipitation there was in the form of graupel or small hail. The hail had slightly negative Z_{DR} values (0 to -0.75 dB), suggesting that it was slightly elongated vertically. Similar observations have been reported by Bringi et al. (1984), Aydin et al. (1984), Balakrishnan and Zrnić (1990), and Hubbert et al. (1998), all at 10-cm wavelength.³

The altitude at which liquid drops started to appear was lower in the hail shaft than in the remainder of the storm, indicating that the particles were relatively large and required a longer time to melt. The variation of Z_{DR}

³ Aydin and Zhao (1990) performed scattering calculations for melting hailstones, which when extrapolated to 3-cm wavelength indicate that negative Z_{DR} values can also be obtained from horizontally elongated hail of large diameter (≈ 15 mm), due to non-Rayleigh effects.

with range through the rain region is shown by the blue trace in the range profile panel; the strongest Z_{DR} value (slightly greater than 2.0 dB) occurred at 31.5-km range, on the far right edge of the main precipitation shaft.

The upper-middle panel shows the phase difference ϕ_{HV} between the H and V components. A “zebra” color palette is used to accentuate small changes in the values (Hooker et al. 1995). In the upper part of the storm ϕ_{HV} was close to 90° , corresponding to LHC polarization. Below 2-km altitude, ϕ_{HV} decreased with range due to the differential propagation phase ϕ_{dp} of rain. The variation of ϕ_{HV} through the rain region is shown by the green (lower) trace in the range profile panel. Because of its cumulative nature, ϕ_{dp} causes ϕ_{HV} to decrease monotonically with range. The fact that ϕ_{HV} increased several times indicates the presence of differential phase upon backscatter, δ_ℓ . The differential backscatter phase is nonzero only when the scatterers are non-Rayleigh and the effects are accentuated here by the relatively short wavelength of the radar ($\lambda = 3.0$ cm). As defined in (6), δ_ℓ has a negative value for horizontally flattened drops and increases the apparent value of ϕ_{dp} at gates containing particles large enough to be in the non-Rayleigh regime. The presence of δ_ℓ is detected only when it goes away, by virtue of an increase in ϕ_{HV} on the far side of a large-particle region. Such opposite-polarity phase changes have been well-documented by other investigators (Bringi et al. 1990; Tan et al. 1991; Holt and Tan 1992; Hubbert et al. 1993), even at 10-cm wavelength. The range profile indicates that ϕ_{HV} increased between 31- and 32-km range, on the far side of the main precipitation shaft, and again on the far side of the storm.

The bottom-middle panel shows the rate of change of ϕ_{HV} with range, or K_{dp} . The values are in degrees per kilometer one-way and were substantially affected by the δ_ℓ effects. (Often K_{dp} is considered to represent the rate of change of differential propagation phase ϕ_{dp} with range, but more generally combines this with the rate of change of δ_ℓ .) Upon entering the strong rain region between 29- and 31-km range along the cursor path, the magnitude of K_{dp} was 3° – 4° km^{-1} or larger. This overestimates the propagation contribution to K_{dp} because of the corresponding increase in δ_ℓ , making the slope of ϕ_{HV} more negative than it would have been otherwise (e.g., Hubbert et al. 1993). The presence of the differential backscatter contribution is indicated by the subsequent increase in ϕ_{HV} , as discussed above. The effect of the increase was to produce large positive K_{dp} values on the far side of the δ_ℓ region, in this case between 31- and 32-km range along the cursor. Therefore δ_ℓ regions are indicated by a couplet of enhanced negative and positive K_{dp} values bracketing the δ_ℓ region. The relative strength of the leading and trailing components of the couplet depends on the suddenness of the δ_ℓ transitions. A particularly strong δ_ℓ couplet occurred just above 2-km altitude between 29- and 30-km range. The values exceeded $\pm 7.5^\circ$ km^{-1} and are in-

dicated by the red-white and blue-white regions at that location. Range profiles through this region (not presented) show that the δ_ℓ excursion was close to -15° . The δ_ℓ region was on the front edge of the main precipitation shaft and was associated with a local maximum of Z_{DR} at the same location. From this and the later observations, the δ_ℓ - Z_{DR} region appeared to be in the storm inflow.

When the δ_ℓ effects are removed to obtain the overall trend of K_{dp} with range, as discussed by Hubbert et al. (1993), the average rate of change of ϕ_{dp} through the rain region was about 16° over 5–6 km, or about 3° km^{-1} two-way (1.5° km^{-1} one way). From the data of Oguchi (1983), this corresponded to an average rainfall rate of 35–40 mm h^{-1} along the path.

The upper-right panel shows the vertical cross section of ρ_{HV} through the storm. The correlation dropped below 0.9 in the precipitation core aloft, indicating the presence of a significant unpolarized component in the backscattered signal.⁴ Such reductions are characteristic of irregularly shaped hail (Balakrishnan and Zrnić 1990). Reduced correlation extended all the way to the ground within the main precipitation region, indicating that the precipitation at lower altitudes consisted of a mixture of rain and hail (e.g., Hubbert et al. 1993, 1998). The profile of ρ_{HV} through the rain region is shown by the black trace in the lower-right panel. Reduced correlation also occurred at 3-km altitude on the front side of the main precipitation shaft, immediately above the strong δ_ℓ region in that location, and in the melting layer on the far side of the storm. The fact that the correlation returned to near-unity values on the far side of the storm indicates that there was not a noticeable propagation effect, and therefore that the unpolarized component was generated during backscatter.

b. Polarization trajectory

A useful way of visualizing the polarization changes is by means of a trajectory on the surface of the Poincaré sphere. A description of the Poincaré sphere is presented in the appendix. Figure 3 shows the trajectory of the polarization state along the radial cursor passing through the rain region of Fig. 2. The Poincaré sphere is shown in projection view from above its north pole, corresponding to LHC (L) polarization. The outermost circle of the projection view corresponds to the equator of the Poincaré sphere and therefore to linear polarizations of varying orientation. Horizontal (H) and vertical (V) polarization are at the bottom and top of the circle, respectively, and $+45^\circ$ and -45° linear polarization are on the right and left sides ($+$, $-$). Polarization states having equal amounts of H and V power correspond to

⁴ From Table A1 of the appendix, a correlation coefficient of 0.9 for incident circular polarization corresponds to a linear depolarization ratio $LDR = -16$ dB.

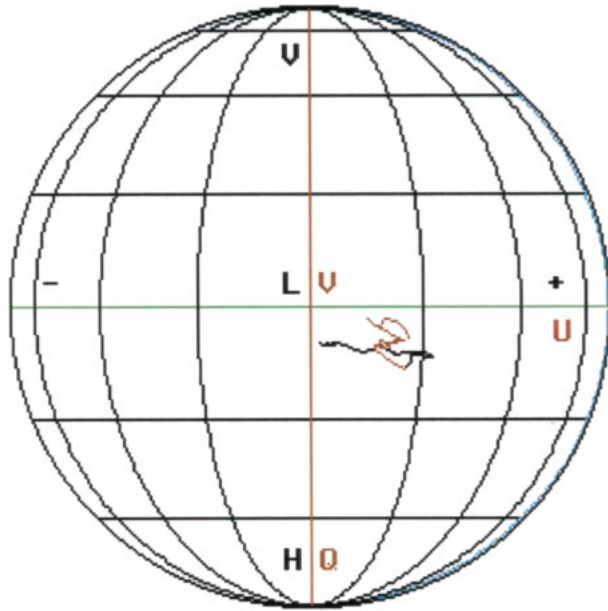


FIG. 3. Trajectory of the polarization state on the surface of the Poincaré sphere, along the radial cursor of Fig. 2. Differential reflectivity Z_{DR} causes the polarization state to be displaced downward along meridional lines, while differential phase effects cause motion to the right, along latitudinal lines (see appendix).

the horizontal line through the center of the projection view. Polarization states below this line have more power in H than in V , and vice versa.

As discussed in the appendix, Z_{DR} values greater than unity enhance the H component of the radar signal relative to the V component and cause the polarization state to be displaced downward below the equal-power line, toward the H polarization point. Differential attenuation (DA) does the opposite, decreasing the horizontal component relative to the vertical and displacing the polarization state upward toward the V polarization point. Differential phase effects (ϕ_{dp} and δ_ϵ) cause the polarization state to move toward the right, namely, from LHC toward $+45^\circ$ polarization. In three dimensions, the differential phase effects cause the polarization state to rotate about the H - V axis of the Poincaré sphere.

The fact that the polarization trajectory in Fig. 3 was entirely below the equal-power line resulted from the differential reflectivity being greater than unity (positive dB values) over the full length of the cursor. The left end of the trajectory was just inside the storm and had already been displaced downward from the transmitted LHC polarization point by positive Z_{DR} . With increasing range the polarization state moved to the right due to differential phase effects, then partially retraced itself upon leaving the δ_ϵ or large-particle region. Along the remainder of the cursor the polarization state gradually returned to the equal power state, but finished to the right of the initial state because of the accumulated differential propagation phase.

The polarization trajectory represents the combined

effects of Z_{DR} and differential attenuation on the one hand and ϕ_{dp} and δ_ϵ on the other hand. The third depolarization process concerns the effect of particle shape variability f and/or random orientation on the correlation coefficient ρ_{HV} . The effect of random variability is to convert some of the polarized power of the radar signal to unpolarized power. The radius of the Poincaré sphere is equal to the polarized power and therefore shrinks as ρ_{HV} decreases, and grows as ρ_{HV} increases. The ratio of the polarized power I_p to the total power I is the degree of polarization p and can be considered to be the normalized radius of the Poincaré sphere. In the appendix it is shown that, when the H and V signal powers are equal or nearly equal, $\rho_{HV} = p$. Thus, reductions in ρ_{HV} cause the radius of the Poincaré sphere to shrink. This effect is not included in the projection view of Fig. 3, but is indicated in Fig. A2 of the appendix. When the H and V powers are equal or nearly equal, the three effects cause the polarization state to change in orthogonal directions on the Poincaré sphere (Scott 1999).

c. Storm evolution

Figures 4 and 5 show vertical scans through the center of the storm at approximately 3-min intervals following the observations of Fig. 2. The scan at 1523:05 (Fig. 4) showed that the reflectivity core had descended and intensified in the lower part of the storm, undoubtedly due to the fall of hail within the core. The ρ_{HV} observations showed that the region of reduced correlation aloft had weakened and did not extend as high in altitude. At the same time, the correlation reductions intensified in the lower part of the precipitation core. Increased negative Z_{DR} values, approaching -1.0 dB, were present in the lower part of the hailshaft, just above the level at which liquid drops started to be detected. As discussed earlier, the hail may have been elongated vertically, in this case due to melting. The strongest correlation reduction occurred in the negative Z_{DR} region, where ρ_{HV} was less than 0.8 ($LDR \cong -13$ dB).

The Fig. 4 data also show that the region of large liquid drops in the inferred inflow region on the near side of the storm had expanded and intensified since the earlier scan, exhibiting a maximum Z_{DR} value of 2.5 dB and a significantly larger spatial extent. A weaker $+Z_{DR}$ maximum was similarly situated on the far side of the core. The K_{dp} results show several regions of coupled negative and positive values, indicative of the effects of δ_ϵ and the presence of large drops. The δ_ϵ regions coincided with local maxima in Z_{DR} , further indicating that the regions contained large drops. The $-Z_{DR}$ maximum in the lower part of the hailshaft was bracketed by a strong K_{dp} couplet of inverse polarity (positive on the near side and negative on the far side), indicating that the hail had an inverse-polarity (i.e., positive) δ_ϵ value, consistent with vertical elongation.

The polarization trajectory through the lower part of

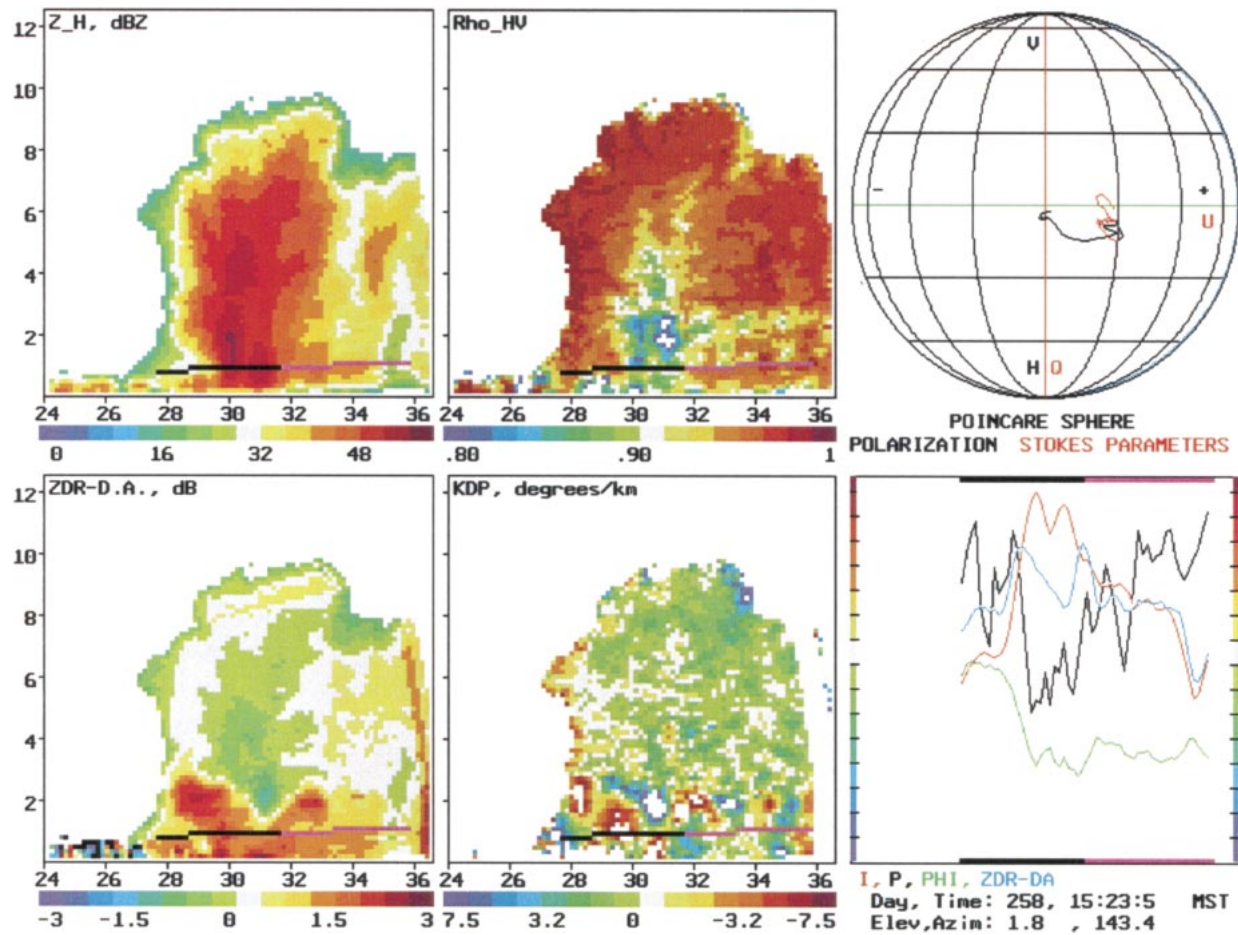


FIG. 4. Vertical cross section at the same azimuth as Fig. 2 but 3 min later, at 1523:05, and showing the polarization trajectory. Note the increased positive Z_{DR} values in the inflow region on the left, the lower altitude at which liquid drops start to appear in the hailshaft, and the enhanced negative Z_{DR} values where the hail would be expected to be melting. The latter region was associated with reductions of ρ_{HV} below 0.80.

the storm exhibited features similar to those of Fig. 3. One difference is that, upon entering the storm, the polarization state changed along a 45° path downward and to the right. This is typical of entering a rain region and reflects the combined effects of increasing Z_{DR} and ϕ_{dp} , whose changes are comparable at 3-cm wavelength on the Poincaré sphere. The upward meandering of the polarization state during the final part of the trajectory is due to the decrease in Z_{DR} on the far side of the storm. At the final gate the H and V powers had returned to nearly equal values, indicating that differential attenuation was not significant.

An additional feature of interest in the Fig. 4 observations is the faint ray of slightly positive Z_{DR} values in the upper part of the storm. This is not an artifact of antenna sidelobes but indicates the presence of electrically aligned ice crystals. Electrical alignment is discussed later; the Z_{DR} artifact occurs because the ice crystals were oriented at an intermediate angle between horizontal and vertical, which caused the the polarization

state to move downward in the projection view, in the same direction as Z_{DR} from liquid drops.

The radar scan at 1526:35 (Fig. 5) showed continued descent and intensification of the precipitation at low levels, and a further decrease in ρ_{HV} below 2-km altitude. Positive Z_{DR} values were no longer seen between the hailshaft and ground, but liquid drops continued to be present throughout much or all of the main precipitation region. This is inferred from the fact that the apparent Z_{DR} values on the far side of the storm were strongly negative (-3 dB), indicating that a significant amount of differential attenuation had occurred in passing through the precipitation. The effect of the differential attenuation is seen in the polarization trajectory, which developed well above the equal-power line along the final part of the range cursor, indicating that the power in H had become substantially less than in V .

The lower part of the hailshaft continued to exhibit negative Z_{DR} values of about -1 dB, by now over a larger, somewhat shallower horizontal region. The fact

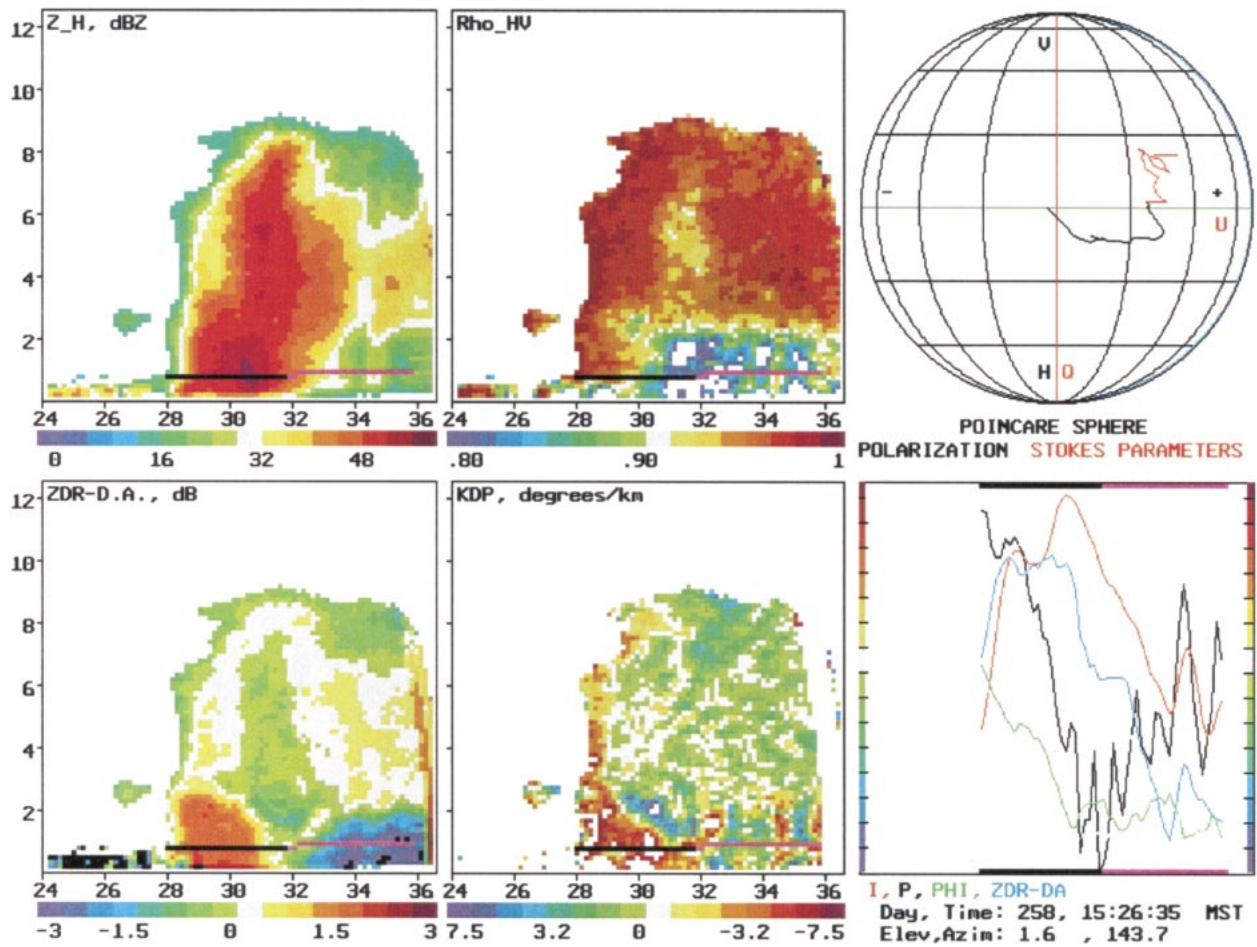


FIG. 5. Same as Fig. 4 but another 3 min later in the storm, at 1526:35. The negative apparent Z_{DR} values below 2-km altitude on the right side of the storm indicate that significant differential attenuation occurred in passing through the main precipitation region. Note the sustained decrease in ρ_{HV} in the same part of the storm, indicating that the radar signal developed an unpolarized component in propagating through the main precipitation region, which by now undoubtedly consisted of mixed hail and rain.

that the negative Z_{DR} region did not extend down to the ground does not mean that the hail had completely melted in the lower altitudes. Rather, any negative Z_{DR} of the hail would tend to have been offset by positive Z_{DR} from liquid drops. The apparent Z_{DR} values were approximately zero in the lower part of the hailshaft, mostly as a result of differential attenuation but possibly also due to the above cancellation effect. As before, inverted polarity K_{dp} values existed on the far side of the melting hail, indicating that the hail produced positive δ_ϵ upon backscatter, consistent with vertical elongation.

From the above, the precipitation in the lower part of the storm was almost certainly mixed phase. This undoubtedly contributed to the large observed reduction in the correlation coefficient. Over large regions ρ_{HV} was below 0.8, and within these regions decreased to as low as 0.70. Of particular significance is the result that the correlation remained low on the far side of the storm. Such “shadowing” is good evidence of a propagation effect; in this case the radar signal developed a sub-

stantial unpolarized component while propagating through the low- ρ_{HV} precipitation core, and accumulated to the level shown. Like ϕ_{dp} , the development of an unpolarized component would be the result of forward scattering, in this case by mixed-phase precipitation having a variety of shapes and orientations, and would be cumulative with range.

d. Signal processing

The above observations were obtained with an inexpensive PC-based digital signal processor (Rison et al. 1993). The processor was originally developed for the Convection and Precipitation/Electrification program in 1991 and used to study the electrical alignment of ice crystals (Chen 1994; Krehbiel et al. 1996). Two Motorola 56001 digital signal processors averaged the signals from 32 transmitted pulses (16 ms at a 2-kHz pulse repetition frequency), at each of 250 1- μ s range gates (37.5-km range). One digital signal processor

(DSP) processed the digitized outputs of matched logarithmic intermediate frequency amplifiers in each receiver channel to obtain W_H and W_V . The other DSP correlated the outputs of coherent, constant-phase amplitude limiters in the two receiver channels to obtain the magnitude and phase of $\hat{\rho}_{HV}$. The 32-pulse averaged data were read into the CPU and stored on disk for postprocessing. To reduce the size of the data files, successive pairs of 32-pulse data were averaged before writing to disk. At the same time the data were processed to produce a real-time display. The results shown in this paper are from postprocessing, but essentially the same software was used to generate the real-time display. The processing further smoothed the data using a running 3-gate (450 m) range average and a 3-ray or angular running average. Since each data ray consisted of the average of (32×2) transmitted pulses to begin with, a total of $9 \times 64 = 576$ samples were averaged. An additional 3-gate running range average was used to smooth the range-differentiated K_{dp} values.

4. Determining particle alignment directions

Nonhorizontal alignment occurs as a result of electrical forces, which orient populations of ice crystals in the direction of the local electric field (Hendry and McCormick 1976; Chen 1994; Metcalf 1995, 1997; Krehbiel et al. 1996). The alignment is detected by the effect that the aligned crystals have on propagation of the radar signal. In particular, the crystals cause cumulative differential propagation phase shift ϕ_{dp} between the components parallel and perpendicular to the alignment direction. Attenuation and differential attenuation can be neglected, even at 3-cm wavelength, because the particles are ice-form. Backscatter effects (Z_{DR} and/or δ_ϵ) from the aligned particles also appear not to be important. Rather, the aligned ice crystals appear to be small and the backscattered signal tends to be dominated by larger hydrometeors (graupel or hail) that serve as a “detector” of the differential phase produced by the aligned crystals (McCormick and Hendry 1979; Hendry and Antar 1982; Krehbiel et al. 1996).⁵

Particles aligned at an angle τ relative to the horizontal depolarize the radar signal in the same manner as horizontal particles, except about an axis of symmetry corresponding to the alignment direction. As discussed in the appendix, the direction of ϕ_{dp} and Z_{DR} changes are rotated by an angle 2τ about the vertical axis of the Poincaré sphere.⁶ Figure 6 illustrates the effect of this

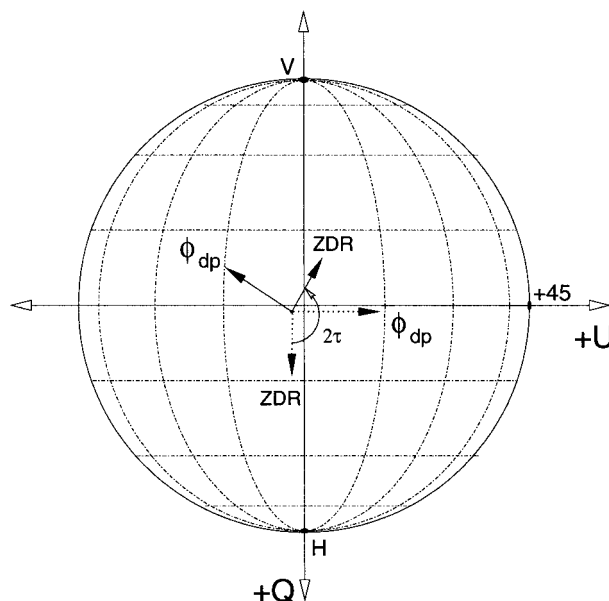


FIG. 6. The polarization changes produced by nonhorizontally aligned particles. The dotted lines indicate the polarization changes produced by horizontally oriented particles; the solid lines show the changes due to particles oriented at an angle τ relative to horizontal.

on the Poincaré sphere projection view of the earlier figures. For vertical orientation, ϕ_{dp} and Z_{DR} would be in the opposite direction from that for horizontal orientation, causing the measured values of ϕ_{dp} and Z_{DR} (dB) to be negative. For particles oriented at $\tau = +45^\circ$, ϕ_{dp} changes would be upward and would be interpreted as negative Z_{DR} values, while positive Z_{DR} would be to the right and interpreted as a ϕ_{dp} effect.

When the depolarization is dominated by differential propagation phase (ϕ_{dp}), the alignment direction is readily determined from the change in the polarization state between successive range gates. Graphically, a line constructed perpendicular to the ϕ_{dp} change in Fig. 6 (i.e., in the Z_{DR} direction), will be oriented at an angle 2τ relative to the H axis. Computationally, the alignment directions are determined by transforming the covariance measurements into the Stokes parameters and using the changes in Q and U to obtain τ (Scott 1999).

Electrical alignment is often vertical or nearly vertical and is observed in the upper and middle part of storms. The electrical nature of the alignment is clearly demonstrated by sudden decreases in the alignment signature at the time of lightning. Vertical orientation comes about only as a result of electrical alignment and is a good indicator of electrification. The result that electric alignment is predominantly vertical agrees well with in situ measurements of the electric field inside storms (e.g., Stolzenburg et al. 1998a,b).

a. Observations

Figures 7 and 8 show examples of electrical alignment from the 15 September storm. The Fig. 7 data are from

⁵ Metcalf (1997) has disputed the point that backscatter effects are not important; full resolution of this question would be obtained by alternately transmitting left- and right-circular polarizations, as discussed later.

⁶ The rotation effect was shown in a series of papers by Barge (1972), McCormick et al. (1972), Humphries (1974), McCormick and Hendry (1975), McCormick and Hendry (1979), and McCormick (1979) using a planar representation of the polarization state.

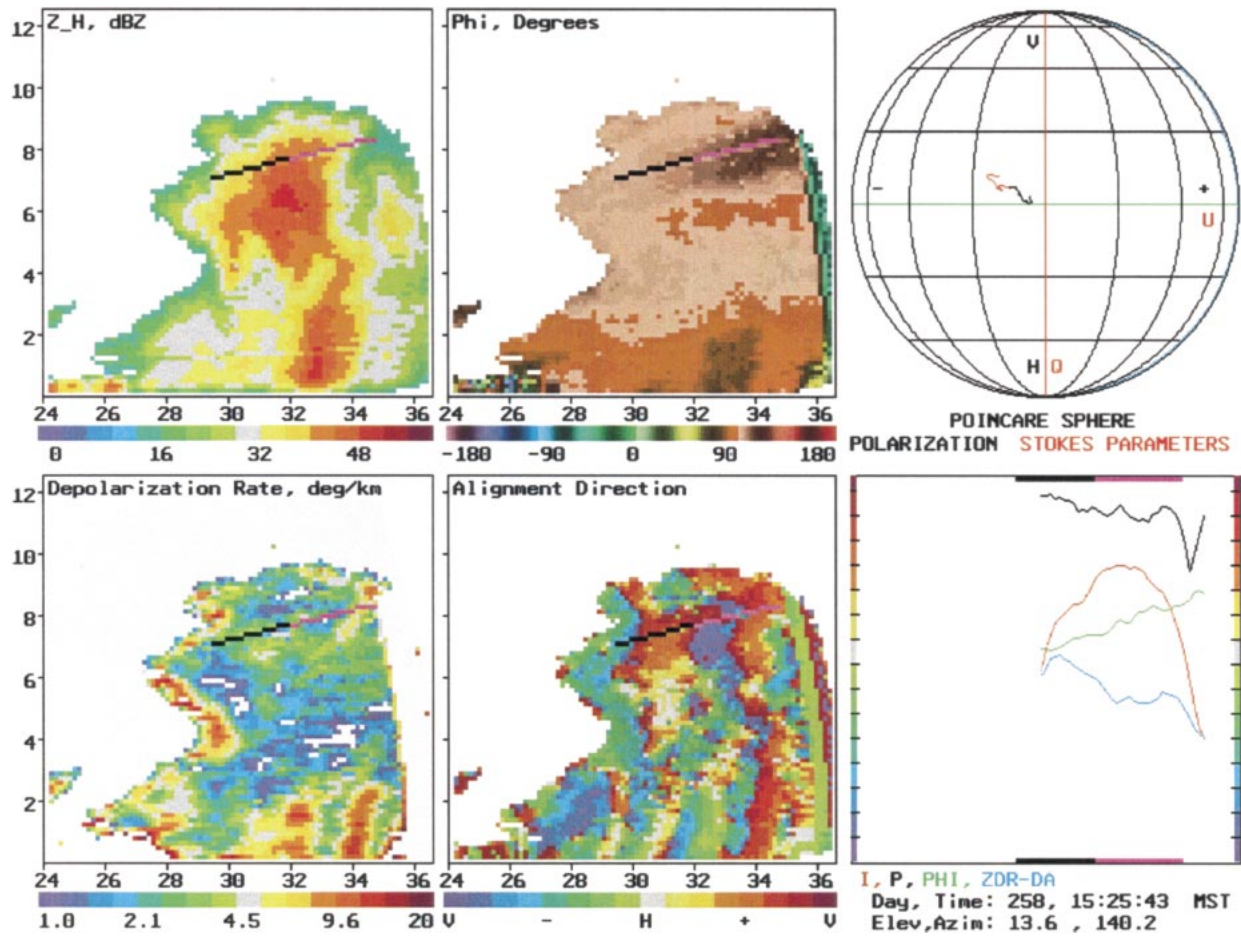


FIG. 7. RHI scan at 1525:43, showing vertical electrical alignment in the upper part of the storm. The alignment is indicated by the dark radial band in the ϕ panel (upper middle) and by the the red-blue region in the alignment direction panel (lower middle).

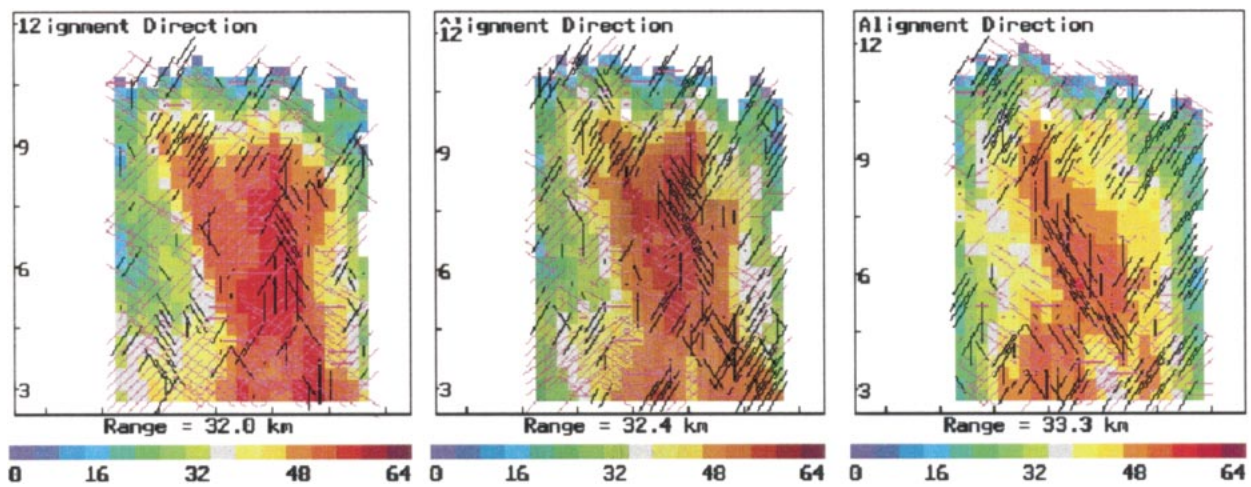


FIG. 8. Alignment direction vectors at three ranges from the radar, reconstructed from a 3D volume scan of the storm between 1524:07 and 1527:18. The observations are on surfaces of constant range from the radar and show the storm as it would be viewed from the radar. Vertical or near-vertical alignment is indicated by the black vectors and shows that strong electrification existed in the upper-left part of the storm, and in the middle-upper part of the main precipitation shaft (see text). The altitudes are in km MSL.

a vertical scan through the northern part of the storm. Electrical alignment caused the correlation phase ϕ_{HV} to increase with range in the upper part of the cloud (dark region, upper-middle panel). The increase is shown by the upward-sloping green line in the range profile panel. From (11) and from the above discussion, this corresponds to a negative value of ϕ_{dp} and hence to vertical orientation. The corresponding polarization trajectory is shown in the Poincaré sphere panel. Differential phase of vertically aligned particles would cause the polarization state to move horizontally to the left with increasing range. The actual motion was to the left and upward, indicating that the alignment was tilted slightly from the vertical.⁷

In a Z_{DR} display the upward component of the polarization trajectory would be interpreted as a radial band of negative Z_{DR} values in the upper part of the storm. This is indicated by the downward-sloping blue line in the range profile panel, and results from the fact that the polarization trajectory extended above the equal-power line in the Poincaré sphere projection view and therefore had more power in V than in H . A similar effect was noted in the upper part of the storm in Fig. 4, but in the Fig. 4 case the Z_{DR} values were slightly positive. In both instances the Z_{DR} values would be real only to the extent that the aligned particles contributed to the backscattered signal; otherwise they are artifacts of differential phase due to alignment that is not fully vertical (or horizontal).

The lower-middle panel of Fig. 7 shows the alignment direction values as a function of position in the storm. Nearly vertical alignment is denoted by the red and blue colors and existed in the upper-middle part of the storm. Such regions are routinely observed to develop and to spread in extent prior to the occurrence of a lightning discharge, and to disappear at the time of the lightning (Krehbiel et al. 1996). The buildup is readily seen in the real-time display and can be used to anticipate when a storm is ready to produce a lightning discharge.

The lower-left panel shows what is termed the depolarization rate. This is the angular rate of change of the polarization state with range; it differs from K_{dp} in that it measures the change of the total spherical angle rather than of just ϕ_{HV} . From the Poincaré sphere plot, the spherical angle changed by about 15° over a distance of about 6 km through the alignment region, corresponding to a two-way depolarization rate of $2.5^\circ \text{ km}^{-1}$. Maximum two-way depolarization rates up to $4.5^\circ \text{ km}^{-1}$ were observed in the electrical alignment region (the green-yellow colors between 6.5- and 8.0-km altitude in the depolarization rate panel). These correspond to regions of significant ice crystal populations, whose presence is revealed by electrical alignment.

The alignment directions are sensed in a plane perpendicular to the radar beam and are best viewed in the perpendicular plane, where they can be represented vectorially. Figure 8 shows the result of doing this. The storm and the alignment directions are seen as they would be viewed from the radar. An individual range-height indicator (RHI) scan provides only a single column of vectors; a complete "map" of alignment directions therefore has to be constructed from contiguous RHI or plan position indicator (PPI) scans, namely, from a volume scan of the storm. The pattern of alignment directions is obtained simultaneously at different ranges, and are shown at 32.0-, 32.4-, and 33.3-km range from the radar. (To avoid having to interpolate the measurements, the alignment directions are shown at a constant range value, corresponding to a spherical rather than a planar surface through the storm.) The background variable is the horizontal reflectivity Z_H at the corresponding ranges. The length of the vectors is proportional to the depolarization rate and indicates the strength of the alignment. For simplicity, the orientation angles are quantized into 22.5° intervals. To accentuate the vertical alignment regions, lines within $\pm 22.5^\circ$ of vertical are in black while the remainder are in magenta. A vector length of one data pixel corresponds to 3° km^{-1} two-way depolarization rate.

The results show two regions of strong vertical alignment. The first was in the upper part of the tilted precipitation shaft at 9-km altitude on the left (north) side of the storm. The data of Fig. 7 are from a vertical scan through the center of this region. The second was at slightly lower altitude (8–9 km MSL) in the reflectivity core. Strong electrification is typically correlated with precipitation at these altitudes (e.g., Krehbiel 1986; Dye et al. 1988).

b. Comments

Many of the indicated alignment directions in the Fig. 8 plots are apparent rather than real. The alignment directions are correct only when the polarization changes are dominated by ϕ_{dp} of aligned particles. This is not the case, for example, in the lower part of the storm, where backscatter effects from liquid drops are important. It is also not the case on the edges of the storm, where the depolarization rate can be artificially high due to signal-to-noise effects. The extent to which the alignment directions are real is not well understood and needs to be further investigated.

As shown by McCormick and Hendry (1975), backscatter and differential phase effects can be separated out from each other by transmitting alternate pulses of LHC and RHC polarization.⁸ The Poincaré sphere rep-

⁷ Alternatively, the alignment could have been exactly vertical and the upward component of the polarization change could have been caused by Z_{DR} from the vertical particles.

⁸ McCormick and Hendry described their results in terms of the normalized cross-covariance W/W_2 [see Eq. (1)]. This represents the

resentation provides a simple way of understanding this; differential phase causes the polarization state to move in the opposite direction at the bottom of the Poincaré sphere (corresponding to RHC polarization), while differential reflectivity changes the polarization state in the same direction. Thus, for example, the polarization trajectory shown in Fig. 7, which was oriented at about 10 o'clock for LHC transmissions, would be oriented at 4 o'clock for RHC transmissions if differential phase effects were dominant, but at 2 o'clock if the particles were vertically oriented and the apparent negative Z_{DR} values were real.

Linearly polarized transmissions can be used to detect electrical alignment when the alignment is vertical or has a significant vertical (or horizontal) component (e.g., Caylor and Chandrasekhar 1996; Zrnić and Ryzhkov 1999). Vertical alignment is detected in the same way as in Fig. 7, namely, by identifying regions of radially extended, opposite-polarity ϕ_{dp} changes. The linear polarization can be transmitted either as alternating pulses of H and V or simultaneously as slant 45° linear. In both cases, particles aligned at $\pm 45^\circ$ are not detected. For 45° transmissions, this is because linearly polarized signals are not depolarized by particles parallel or perpendicular to the plane of polarization. For alternating pulse transmissions, it is because the H and V signals are equally depolarized by particles oriented at $\pm 45^\circ$. Alternating H and V transmissions therefore simulate a 45° linear transmitted signal from the standpoint of detecting aligned particles. Both types of transmissions detect alignment only when it has a significant horizontal or vertical component. One can distinguish the "sign" of the alignment (horizontal or vertical) but the actual alignment directions cannot be determined.

Circularly polarized transmissions detect all alignment directions equally well, by virtue of the fact that the depolarization is independent of particle orientation. In addition, the alignment directions can be determined.

5. Summary and discussion

Linear polarization quantities such as Z_{DR} , ϕ_{dp} , and ρ_{HV} are readily determined by transmitting H and V polarizations simultaneously and by measuring the back-scattered returns in parallel H and V receiving channels. The measurements are improved over those obtained when H and V are transmitted on alternate pulses be-

cause the dual-polarization quantities are determined from simultaneous rather than from pulse-to-pulse measurements.

The advantages of transmitting H and V simultaneously are summarized as follows.

1) Because they are not contaminated by Doppler effects, ϕ_{dp} and ρ_{HV} have less uncertainty. The variance introduced by the pulse-to-pulse Doppler shift can be a significant source of uncertainty in alternating pulse measurements. It is important that the variance be minimized because the desired effects tend to be relatively weak, especially at longer wavelengths.

2) The measurements are speeded up by at least a factor of 2 because signal estimates are obtained from each transmitted pulse rather than from pairs of pulses. Also, the dwell time needed to achieve a given variance is decreased because one does not need to average out the Doppler effects.

3) A high-power polarization switch is not needed; it is replaced by a power divider. Dual receiving channels are required, but modern receiving techniques makes this relatively easy to implement in a highly matched manner. Optimal signal-to-noise ratios are maintained in both receiver channels, as in the alternating pulse technique. (The signal-to-noise values are up to 3 dB lower than those of alternating pulse returns because the transmitted power is divided between the two polarizations rather than switched entirely into one polarization or the other.)

4) The relative phases of the H and V components can be adjusted to transmit circular or 45° linear polarization. As discussed below, circular polarization is more sensitive to the presence of randomly oriented particles. Circular polarization also enables particle alignment directions to be determined, if desired. Alignment observations can be used to detect and study the electrification of storms and also provide a way of remotely sensing ice crystal populations in electrified storms.

5) The time saved by not having to alternate between H and V polarizations can be used to obtain true polarization diverse measurements, for example, by alternating between LHC and $+45^\circ$ linear polarizations, to aid in particle identification.

Many of the above advantages have been recognized by previous investigators, as summarized in the introduction. The advantages have also been recognized in a recent study by Doviak et al. (2000), who proposed that simultaneous transmissions be used for polarimetric upgrades of the NEXRAD weather radars.

The simultaneous transmission approach has been illustrated with observations from a 3-cm wavelength radar, but the formulations and concepts are general and apply to any wavelength. The 3-cm measurements have the advantage of being relatively sensitive to differential phase effects, both during propagation and backscatter. But they can be significantly affected by attenuation and by differential attenuation in liquid precipitation. The

polarization state in a 2D plane, corresponding to the real and imaginary parts of W/W_2 . Scott (1999) has shown that the W/W_2 representation corresponds to a stereographic projection of the polarization state onto a plane tangent to the Poincaré sphere at the LHC (or RHC) polarization point. Such a projection becomes increasingly nonlinear as the polarization state departs from circular, making analytical formulations intractable for all but small depolarizations. In addition, the representation is nonconformal, as the 3D polarization state is described in two dimensions. The Poincaré sphere representation eliminates these problems.

latter can bias Z_{DR} values strongly negative, as seen, for example, in the data of Fig. 5. Differential attenuation is usually not a problem at 10-cm wavelength, but can be significant when passing through extensive rain regions (Zrnić and Ryzhkov 1999). For this reason differential propagation phase ϕ_{dp} is considered to be a more robust measure of liquid precipitation rates in storms (e.g., Zrnić and Ryzhkov 1996). Differential propagation phase is weaker at 10-cm than at 3-cm wavelength but is less affected by differential phase upon backscatter, δ_ϵ . The δ_ϵ effects can dominate specific differential phase (K_{dp}) values at 3-cm wavelength, as seen, for example, in Figs. 2 and 4.

With the contaminating Doppler effects removed by simultaneous measurements, the uncertainties in Z_{DR} , ϕ_{HV} , and ρ_{HV} are limited by their fundamental variances. For example, from Bendat and Piersol (1986), the standard deviation for differential phase measurements is [their Eq. (9.52)]

$$\sigma_\phi = \frac{1}{\sqrt{N}} \frac{\sqrt{1 - \rho^2}}{\sqrt{2\rho}}, \quad (15)$$

where N is the number of independent samples being averaged and ρ is the H - V correlation coefficient. Here σ_ϕ depends only on ρ and approaches zero as ρ approaches unity. For $N = 64$ samples, the rms uncertainty in ϕ is 1.0° for $\rho_{HV} = 0.98$ and 2.5° for $\rho_{HV} = 0.90$. These values are comparable to the rate of change of ϕ_{dp} with range, which is a few degrees per kilometer or less, highlighting the importance of minimizing the variance. Corresponding expressions for the variance of ρ and Z_{DR} have been determined by Schultz and Kostinski (1997) for the simultaneous transmission case.

The relative virtues of transmitting circular and 45° linear polarization are as follows: Both types of transmissions are equally depolarized by horizontally oriented particles such as rain. The only difference is the initial value of the phase difference ϕ_{HV} . The same is true for scattering by vertically oriented particles. For particles aligned at an intermediate angle between horizontal and vertical, the polarization changes are less for linear than for circular polarization. This is because the depolarization of circular radiation is independent of particle orientation, while that of linear radiation is a minimum when the particles are parallel or perpendicular to the direction of polarization. One result of this, discussed in the previous section, is that linear transmissions are able to detect whether alignment has a vertical or horizontal component, but not the actual alignment direction.

Similarly, the depolarization produced by randomly oriented particles is different for circular and linear incident polarization. Some of the particles tend to be aligned with linear polarization (of any orientation), causing the linear radiation to be depolarized less than circular. For both polarizations, the effect of random orientation is to convert some of the incident polarized

power to unpolarized power. This reduces both the degree of polarization p of the radar signal and the correlation coefficient ρ of the orthogonal returns. (Variability in the shape of aligned particles has the same effect, through the parameter f .) As shown in the appendix, $\rho_{HV} = p$ when the incident H and V powers are equal or nearly equal. Circular and 45° linear polarization have equal H - V powers, and alternate H and V transmissions approximate the equal power state. In all cases, ρ_{HV} measures p and hence the presence of an unpolarized component. The fact that ρ_{HV} and p are closely related was noted by Torlaschi and Holt (1998); the details of the relationship are described in the appendix.

Scott (1999) has shown that the depolarization caused by randomly oriented particles is a function only of the scattering parameter

$$g = \frac{4\text{Re}\{\langle S_{xx}S_{yy}^* \rangle\}}{\langle |S_{xx} + S_{yy}|^2 \rangle}, \quad (16)$$

where S_{xx} and S_{yy} are the major and minor axes scattering cross sections of the particles. Here g measures the departure of the particles from sphericity, being unity when the particles are spherical and reducing to zero for highly elongated particles such as chaff. Therefore g is termed the sphericity parameter. It is analogous to the shape correlation factor f of horizontally aligned particles and is a function of Z_{DR} , f , and δ_ϵ that the particles would have if they were aligned.⁹ As shown by Scott, the effect of random orientation is to reduce the degree of polarization by a factor of $g/(2 - g)$ when the incident polarization is circular, and by $1/(2 - g)$ when the incident polarization is linear. For g close to unity, it can be shown that the reduction in p (and hence in ρ_{HV}) is a factor of two greater for circular polarization than for linear polarization. For larger decreases of g below unity, the difference is greater than a factor of two (see Table A1).

Summarizing, circular polarization is equivalent to linear polarization (either 45° linear or alternating H and V transmissions) for sensing horizontally oriented particles such as rain. Linear and circular polarizations respond differently to particles oriented at intermediate angles between H and V , with circular polarization being optimal for detecting both randomly oriented particles and aligned particles of arbitrary orientation. If one is able to transmit only a single polarization, the optimal choice would be circular. The same conclusion was reached by Torlaschi and Holt (1998), who determined that of the three primary polarizations (circular, 45° lin-

⁹ In particular,

$$g = \frac{4}{2 + \frac{1}{f \cos \delta_\epsilon} \left(\sqrt{Z_{DR}} + \frac{1}{\sqrt{Z_{DR}}} \right)}$$

ear, and horizontal/vertical), circular polarization is optimal for meteorological observations. Their study considered the returns to be measured in the same basis as the transmitted signals, but the signals are best received in an H - V basis.¹⁰

The fact that circular and 45° linear polarizations are affected differently by horizontal and randomly oriented particles means that polarization diverse measurements, in which the transmitted signal is alternated between circular and 45° linear polarization, in principle provide a means of separating out the contributions of the two classes of particles. Alternatively, switching between LHC and RHC polarization would enable alignment directions to be determined in the presence of backscatter effects, as discussed in section 4. The simultaneous transmission approach makes such observations practical because one does not have to alternate between H and V transmissions. The switching would be implemented using an electronic phase shifter rather than a polarization switch.

The linear depolarization ratio (LDR) continues to be considered an important quantity in dual-polarization observations (e.g., Hubbert et al. 1998; Zrnić and Ryzhkov 1999). It is determined by transmitting either horizontal or vertical polarization and by measuring the returns in H and V receiving channels. The simultaneous transmission technique, implemented in an H - V basis, does not allow LDR to be measured unless a switchable attenuator (or an actual switch) were included in one of the power divider channels.

LDR senses two aspects of the precipitation: random orientation or irregular shapes, and nonhorizontal (or nonvertical) orientation, due, for example, to canting or electrical alignment. In the appendix it is shown that the information that LDR provides on randomly oriented particles is exactly the same as that provided by ρ_{HV} from simultaneous transmissions. In both cases, what is being detected is the effect of the scatterers on the degree of polarization p . LDR measures p by virtue of the contribution of the unpolarized part of the signal to the cross-polar power. The correlation coefficient ρ_{HV} measures p by the effect of the unpolarized component on the signal correlation. The different quantities are related according to

$$\text{LDR} = \frac{1 - p}{1 + p} \quad (17)$$

$$\rho_{HV} = \frac{1 - \text{LDR}}{1 + \text{LDR}}. \quad (18)$$

¹⁰ Circular polarization returns could be received in another linear basis and transformed to an H - V basis for determining those parameters. This was in fact done in the observations of this study to correct for a 9.5° tilt in the antenna's orthomode polarization transducer from true horizontal and vertical. Similar transformations could be applied to signals received in a circular polarization basis, as discussed by Jameson and Davé (1988), although the effects of unequal signal-to-noise ratios on the transformations would need to be determined.

Mead et al. (1993) and Tang and Aydin (1995) investigated the random orientation case and obtained the same relation between LDR and p , but a different relation between ρ_{HV} and LDR. The relation obtained by these and other investigators is $\rho_{HV} = 1 - 2\text{LDR}$. The apparent discrepancy is resolved by noting that ρ_{HV} is different in the two expressions (V.N. Bringi and V. Chandrasekar 2000, personal communication). In particular, $\rho_{HV} = 1 - 2\text{LDR}$ refers to the copolar-copolar correlation of alternating H and V transmissions [i.e., $\rho_{HV}(0)$], while ρ_{HV} of (18) is from simultaneous transmissions. The difference is described in more detail in the appendix.

The above relations assume LDR is not affected by canting of aligned particles. Because canting can affect LDR, and because LDR is an incoherently measured quantity, ρ_{HV} should provide a better measure of randomly oriented particles than LDR. This may not be true for $\rho_{HV}(0)$ obtained from alternating H and V transmissions, due to the uncertainties of estimating $\rho_{HV}(0)$ from $\rho_{HV}(T)$. But it should be true for ρ_{HV} values determined from simultaneous transmissions. In this case, the only additional information provided by LDR concerns the presence of canting. If the canting information is not important or is not needed, LDR does not need to be measured. For radars in which the correlation coefficient is not measured, LDR is a surrogate for ρ_{HV} .

Acknowledgments. This study was the subject of a Ph.D. dissertation by one of the authors (Scott 1999). The authors are deeply indebted to Steve McCrary (deceased) for his dedicated work on the dual-polarization radar. The work was supported in part by the U.S. Air Force Office of Scientific Research, under Grants AFOSR-89-0450, F49620-92-J-0320 (AASERT), and F49620-96-1-0304. Partial support was also provided by the New Mexico Universities Collaborative Research Program (NUCOR) of Los Alamos National Laboratory. The authors thank the reviewers for their constructive comments, and A.R. Holt for his stimulating discussions and for providing results from his studies. We also thank V.N. Bringi and V. Chandrasekar for their assistance in resolving the discrepancy in the ρ_{HV} -LDR relations.

APPENDIX

The Poincaré Sphere Representation

Figure A1 shows the Poincaré sphere in three spatial dimensions. The north and south poles of the sphere correspond to left- and right-hand circular polarizations, respectively, while the equator corresponds to linear polarization of varying orientation angle. Horizontal and vertical polarization are at the front and back of the sphere, while $\pm 45^\circ$ polarizations are on the right and left sides.

The Stokes parameters Q , U , and V constitute the Cartesian coordinates of the sphere. Each Stokes pa-

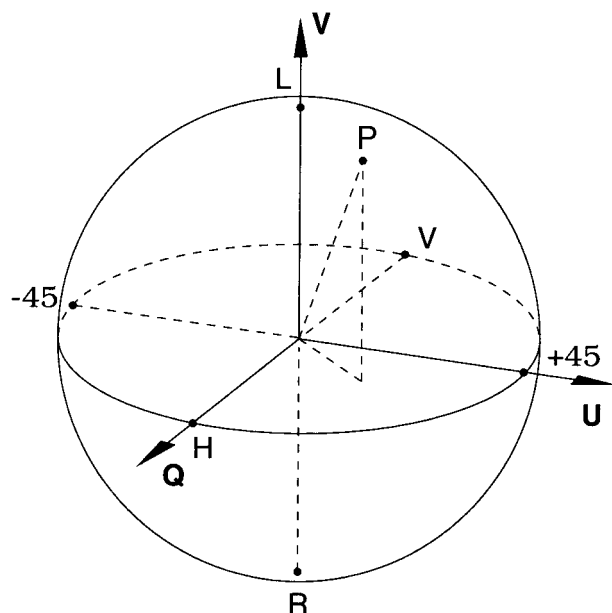


FIG. A1. The Poincaré sphere and Stokes coordinate system, showing the location of horizontal (H) and vertical (V) polarizations, left- and right-hand circular (L/R), and $\pm 45^\circ$ slant linear polarizations. The point P represents a given polarization state and lies on the surface of the sphere. The radius of the sphere corresponds to the total polarized power, which, when normalized to the total power, corresponds to the degree of polarization p .

parameter corresponds to the difference in the orthogonal powers of the associated basis; thus, $Q = W_H - W_V$. From the study by Scott (1999), differential reflectivity of liquid drops increases W_H relative to W_V , thereby increasing Q and moving the polarization state toward the H polarization point. Differential attenuation by liquid drops (DA) does the opposite and moves the polarization state toward the V polarization point. These effects are illustrated in Fig. A2. The angle ϕ in Fig. A2 corresponds to the phase difference between the H and V components and is the same as ϕ_{HV} . Differential phase effects change ϕ_{HV} according to (11) and cause the polarization state to change in a direction parallel to the U - V plane. When LHC polarization is transmitted, ϕ_{dp} of liquid drops decreases ϕ and causes the polarization state to move toward $+45^\circ$ linear. As discussed in the text, δ_t has a negative sign for horizontally oriented drops and causes ϕ to change in the same direction as ϕ_{dp} .

Nonunity values of f due to particle shape variability introduce an unpolarized component in the radar signal and reduce the degree of polarization p . The degree of polarization is the ratio of the polarized power to the total signal power and represents the radius of the Poincaré sphere when the total power is normalized to unity. In the next section, we show that $p = \rho_{HV}$ when the radar signal contains equal or nearly equal H and V powers. This occurs when the polarization state is in the vicinity of the U - V plane, that is, on or near the

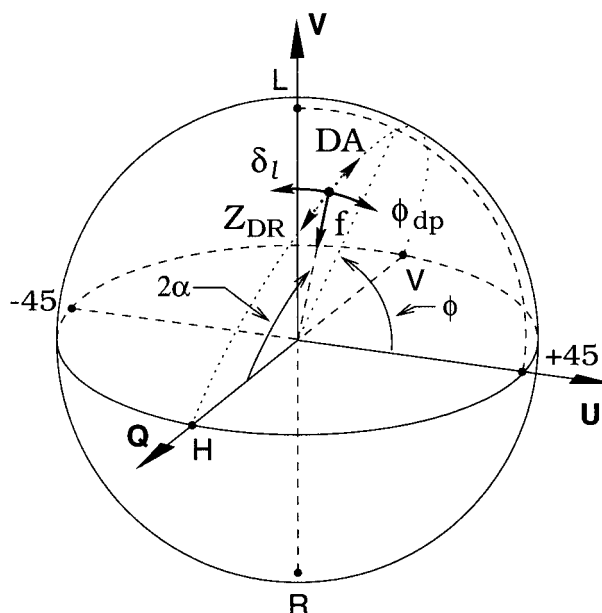


FIG. A2. The polarization changes produced by horizontally aligned particles, and the (α, ϕ) spherical coordinate system in which the changes are best described.

great circle passing through the circular and 45° polarization points. It is the normal situation for simultaneous transmissions and is also the situation simulated by alternating H and V transmissions. Near the equal-power circle, nonunity values of f change the polarization state in a radial direction and reduce the diameter of the Poincaré sphere. The three types of polarization changes (differential phase, differential reflectivity and attenuation, and shape variability) are therefore in orthogonal directions. Further, for horizontally oriented particles, the changes are rotationally symmetric about the Q or H axis of the Poincaré sphere.

Particles that are not horizontally oriented depolarize the radar signal in the same way as above, except about an axis of symmetry Q' corresponding to the alignment direction. This is illustrated in Fig. A3. For particles oriented at an angle τ relative to the horizontal, Q' is rotated an angle 2τ away from Q in the linear polarization plane. The polarization changes are rotated by the same amount when viewed in projection from above the sphere, as in Fig. 6. The depolarization by particles having a range of canting angles about a given direction can be represented as the superposition of slightly rotated polarization changes.

Randomly oriented particles change the polarization state in a manner that is rotationally symmetric about the vertical axis of the Poincaré sphere, namely, the Stokes V axis. This can be seen from the fact that the depolarization of linear radiation is independent of the polarization direction, and hence of the location of the polarization state around the equator of the Poincaré sphere. The polarization changes produced by horizontal

Relation between LDR and ρ_{HV} for Randomly Oriented Scatterers

The linear depolarization ratio LDR detects the presence of randomly oriented particles and departures from horizontal (or vertical) alignment, due, for example, to canting. In both instances, some of the incident or copolar power (e.g., W_H) is converted to cross-polar or orthogonal power (W_V) due to the fact that some or all of the particles are not oriented parallel or perpendicular to the incident polarization. The effect of random orientation is to introduce an unpolarized component in the scattered signal, thereby decreasing the degree of polarization p . Aligned particles that are canted from horizontal or vertical generate polarized cross-polar power due to the effect of the particles' Z_{DR} on the incident polarization state.^{A1}

If canting is not important, LDR measures the presence of randomly oriented or shaped particles, and therefore detects changes in p . LDR and p are related, as shown below.

Assuming the transmitted signal is horizontally polarized, LDR is defined to be the ratio of the power received in the cross-polar channel (V) to that received in the copolar channel (H). Namely,

$$\text{LDR}|_H = \frac{W_V}{W_H}. \quad (\text{A8})$$

In general, W_H and W_V are the sum of the polarized and unpolarized powers in each of the polarizations,

$$W_H = E_H^2 + E_u^2, \quad W_V = E_V^2 + E_u^2, \quad (\text{A9})$$

where E_H^2 and E_V^2 are the powers of the polarized components of the signal and E_u^2 is the unpolarized power, which is equal in both polarizations. When only H is transmitted and the scattering is by randomly oriented particles, the cross-polar or V return has only an unpolarized component. Thus, $E_V^2 = 0$ and

$$\text{LDR}|_H = \frac{E_u^2}{E_H^2 + E_u^2}. \quad (\text{A10})$$

Similarly, the degree of polarization is given by

$$p = \frac{E_H^2 + E_V^2}{E_H^2 + E_V^2 + 2E_u^2}, \quad (\text{A11})$$

which, with $E_V^2 = 0$, becomes

$$p = \frac{E_H^2}{E_H^2 + 2E_u^2}. \quad (\text{A12})$$

Equations (A10) and (A12) can be expressed in terms of the ratio E_u^2/E_H^2 and solved to show that

$$\text{LDR}|_{H,V} = \frac{1-p}{1+p}. \quad (\text{A13})$$

Thus, LDR is a bilinear transformation of p . The same result is obtained if LDR is determined from V transmissions; hence the subscript H, V . When the particles are spherical, $p = 1$ and $\text{LDR} = 0$. Inversely,

$$p = \frac{1 - \text{LDR}|_{H,V}}{1 + \text{LDR}|_{H,V}}. \quad (\text{A14})$$

Mead et al. (1993) and Tang and Aydin (1995) obtained the same result using a Mueller matrix formulation for randomly oriented scatterers.

The above shows how LDR measures the effect of randomly oriented particles on p , and holds only when LDR is determined from H or V transmissions. Also, p is the degree of polarization for incident linear radiation.

Scott (1999) has shown that, for randomly oriented scatterers illuminated by linear radiation, the degree of polarization of the scattered signal is reduced from its incident value $p|^i$ to

$$p|^s = \frac{1}{(2-g)}p|^i, \quad (\text{A15})$$

where g is the sphericity parameter given in (16). Expressing LDR in terms of g , and assuming the incident signal to be fully polarized,

$$\text{LDR}|_{H,V} = \frac{(1-g)}{(3-g)}. \quad (\text{A16})$$

For highly elongated scatterers such as chaff, $g = 0$ and p is reduced by a factor of $1/2$. LDR for the scatterers is $1/3$, or -4.77 dB. This represents the maximum amount that linear radiation can be depolarized by randomly oriented scatterers. (By contrast, circular radiation is completely unpolarized by highly elongated scatterers.) Equation (A16) can also be obtained from direct analysis of the random orientation problem.

The reduction in p for linear incident polarization can be determined not only from LDR but more directly by measuring ρ_{HV} . The correlation coefficient ρ_{HV} can be measured from 45° linear or alternating H and V transmissions. For 45° transmissions, we have from (A5) that $\rho_{HV} \equiv p$, so that

$$\text{LDR}|_{H,V} = \frac{1 - \rho_{HV}|_{45}}{1 + \rho_{HV}|_{45}}. \quad (\text{A17})$$

Inversely,

$$\rho_{HV}|_{45} = \frac{1 - \text{LDR}|_{H,V}}{1 + \text{LDR}|_{H,V}}. \quad (\text{A18})$$

Thus, ρ_{HV} from 45° linear transmissions provides the same information as LDR.

For alternating transmissions, $\rho_{HV}(0)$ differs from ρ_{HV} when the scatterers are canted from horizontal or vertical. This is because canted scatterers couple some of the V transmitted power of simultaneous transmissions

^{A1} In the geometric representation of Fig. A3, aligned particles oriented at an angle τ will cause an incident H polarization to move from the Q or H polarization point toward the Q' point, thereby reducing $Q = W_H - W_V$.

TABLE A1. Effect of the sphericity parameter g of randomly oriented scatterers on the radar measurables.

g	0.99	0.98	0.95	0.90	0.80
LDR (dB)	-23.0	-20.0	-16.1	-13.2	-10.4
$\rho_{HV}(0)$	0.990	0.980	0.951	0.905	0.818
$\rho_{HV} _{45}$	0.990	0.980	0.952	0.909	0.833
$\rho_{HV} _{L,R}$	0.980	0.961	0.905	0.818	0.667

into the H channel that is not present when only H is transmitted, and vice versa (e.g., Seliga and Bringi 1976; Sachidananda and Zrnić 1985; Doviak et al. 2000). The difference is greatest when the scatterers are randomly oriented. In this case, and when the incident polarization is completely polarized, it can be shown that

$$\rho_{HV}(0) = \frac{(1 + g)}{(3 - g)}. \quad (A19)$$

This compares with

$$\rho_{HV}|_{45} = \frac{1}{(2 - g)} \quad (A20)$$

for slant 45° transmissions. Using (A16) to express $\rho_{HV}(0)$ in terms of LDR gives

$$\rho_{HV}(0) = 1 - 2\text{LDR}|_{H,V}. \quad (A21)$$

This is the result obtained by Mead et al. (1993) and by Tang and Aydin (1995). It differs from (A18) because $\rho_{HV}(0)$ is determined from separate rather than simultaneous transmissions. Since $(1 - \text{LDR})/(1 + \text{LDR}) \cong 1 - 2\text{LDR}$ for small LDR, $\rho_{HV}|_{45}$ and $\rho_{HV}(0)$ are essentially equal for weak depolarization values.

Depending on how the measurements are made, the sphericity parameter g can be determined from (A16), (A19), or (A20). Alternatively, if the incident polarization is circular, g can be determined from the analogous result to (A15),

$$p|^s = \frac{g}{(2 - g)} p|^i = \rho_{HV}|_{L,R}. \quad (A22)$$

Table A1 gives numerical values of the different measurables versus g . For small depolarizations, $\rho_{HV}|_{45} \cong \rho_{HV}(0) \cong g$.

Mead et al. (1993) and Tang and Aydin (1995) showed that the scattering by randomly oriented particles is characterized by a single parameter, which they considered to be LDR. The more fundamental quantity characterizing the scatterers is g . Expressing the elements of the Mueller matrix from Tang and Aydin (1995) in terms of g , one obtains for the Stokes transformation that

$$\begin{bmatrix} I \\ Q \\ U \\ V \end{bmatrix}^s = A \begin{bmatrix} 1 & 0 & 0 & 0 \\ 0 & \frac{1}{2 - g} & 0 & 0 \\ 0 & 0 & \frac{1}{2 - g} & 0 \\ 0 & 0 & 0 & \frac{g}{2 - g} \end{bmatrix} \begin{bmatrix} I \\ Q \\ U \\ V \end{bmatrix}^i, \quad (A23)$$

where $A = \frac{1}{2}[\langle |S_{xx}|^2 \rangle + \langle |S_{yy}|^2 \rangle]$ is the average scattering cross section of the particles. The diagonal elements corresponding to Q , U , and V are the same as the reduction in the degree of polarization for linear and circular incident polarizations.

REFERENCES

Aydin, K., and Y. Zhao, 1990: A computational study of polarimetric radar observables in hail. *Geosci. Remote Sens.*, **28**, 412–422.

———, T. A. Seliga, and V. N. Bringi, 1984: Differential radar scattering properties of model hail and mixed phase hydrometeors. *Radio Sci.*, **19**, 58–66.

Balakrishnan, N., and D. S. Zrnić, 1990: Use of polarization to characterize precipitation and discriminate large hail. *J. Atmos. Sci.*, **47**, 1525–1540.

Barge, B., 1972: Hail detection with a polarization-diversity radar. Stormy Weather Group Sci. Rep. MW-71, McGill University, 80 pp. [Available from Physical Sciences and Engineering Library, McGill University, 809 Sherbrooke St. West, Montreal, PQ H3A 2K6, Canada.]

Bendat, J. S., and A. G. Piersol, 1986: *Random Data: Analysis and Measurement Procedures*. John Wiley and Sons, 566 pp.

Born, M., and E. Wolf, 1975: *Principles of Optics*. Pergamon Press, 808 pp.

Bringi, V. N., and A. Hendry, 1990: Technology of polarization diversity radars for meteorology. *Radar in Meteorology*, David Atlas, Ed., Amer. Meteor. Soc., 153–190.

———, T. A. Seliga, and K. Aydin, 1984: Hail detection with a differential reflectivity radar. *Science*, **225**, 1145–1147.

———, V. Chandrasekar, N. Balakrishnan, and D. Zrnić, 1990: An examination of propagation effects in rainfall on radar measurements at microwave frequencies. *J. Atmos. Oceanic Technol.*, **7**, 829–840.

———, P. Meischner, J. Hubbert, and Y. Golestani, 1991: Polarimetric radar signatures of precipitation at S- and C-bands. *Proc. IEEE-F*, **138**, 109–119.

Brunkow, D., P. Kennedy, S. Rutledge, V. Bringi, and V. Chandrasekar, 1997: CSU-Chill radar status and comparison of available operating modes. Preprints, *28th Conf. on Radar Meteorology*, Austin, TX, Amer. Meteor. Soc., 43–44.

———, V. N. Bringi, P. C. Kennedy, S. A. Rutledge, V. Chandrasekar, E. A. Mueller, and R. K. Bowie, 2000: A description of the CSU-CHILL National Radar Facility. *J. Atmos. Oceanic Technol.*, **17**, 1596–1608.

Caylor, I., and V. Chandrasekar, 1996: Time-varying ice crystal orientation in thunderstorms observed with multiparameter radar. *Geosci. Remote Sens.*, **34**, 847–858.

Chen, T., 1994: Radar detection of electrically aligned particles in thunderstorms. Ph.D. thesis, New Mexico Institute of Mining and Technology, 198 pp. [Available from NMIMT Library, 801 Leroy St., Socorro, NM 87801.]

Doviak, R., and D. Zrnić, 1993: *Doppler Radar and Weather Observations*. Academic Press, 562 pp.

———, V. Bringi, A. Ryzhkov, A. Zahrai, and D. Zrnić, 2000: Considerations for polarimetric upgrades to operational WSR-88D radars. *J. Atmos. Oceanic Technol.*, **17**, 257–278.

- Dye, J., J. Jones, A. Weinheimer, and W. Winn, 1988: Observations within two regions of charge during initial thunderstorm electrification. *Quart. J. Roy. Meteor. Soc.*, **114**, 1271–1290.
- Hall, M. P. M., S. M. Cherry, J. W. F. Goddard, and G. R. Kennedy, 1980: Raindrop sizes and rainfall rate measured by dual-polarization radar. *Nature*, **285**, 195–198.
- , J. W. F. Goddard, and S. M. Cherry, 1984: Identification of hydrometeors and other targets by dual-polarization radar. *Radio Sci.*, **19**, 132–140.
- Hendry, A., and G. McCormick, 1976: Radar observations of alignment of precipitation particles by electrostatic fields in thunderstorms. *J. Geophys. Res.*, **81**, 5353–5357.
- , and Y. M. M. Antar, 1982: Radar observations of polarization characteristics and lightning-induced realignment of atmospheric ice crystals. *Radio Sci.*, **17**, 1243–1250.
- Holt, A., and J. Tan, 1992: Separation of differential propagation phase and differential backscatter phase in polarization diversity radar. *Electron. Lett.*, **28**, 943–944.
- , V. N. Bringi, and D. Brunkow, 1999: A comparison between parameters obtained with the CSU-CHILL radar from simultaneous and switched transmission of vertical and horizontal polarization. Preprints, *29th Int. Conf. on Radar Meteorology*, Montreal, PQ, Canada, Amer. Meteor. Soc., 214–217.
- Hooker, S., J. Brown, and A. Kirwan Jr., 1995: Detecting “dipole ring” separatrixes with zebra palettes. *Geosci. Remote Sens.*, **33**, 1306–1312.
- Hubbert, J., V. Chandrasekar, V. Bringi, and P. Meischner, 1993: Processing and interpretation of coherent dual-polarized radar measurements. *J. Atmos. Oceanic Technol.*, **10**, 155–164.
- , V. Bringi, L. Carey, and S. Bolen, 1998: CSU-CHILL polarimetric radar measurements from a severe hail storm in eastern Colorado. *J. Appl. Meteor.*, **37**, 749–775.
- Humphries, R., 1974: Depolarization effects at 3 GHz due to precipitation. Stormy Weather Group Sci. Rep. MW-82, McGill University, 84 pp. [Available from Physical Sciences and Engineering Library, McGill University, 809 Sherbrooke St. West, Montreal, PQ H3A 2K6, Canada.]
- Illingworth, A. J., and I. J. Caylor, 1991: Co-polar correlation measurements of precipitation. Preprints, *25th Int. Conf. on Radar Meteorology*, Paris, France, Amer. Meteor. Soc., 650–653.
- Jameson, A. R., 1983: Microphysical interpretation of multi-parameter radar measurements in rain. Part I: Interpretation of polarization measurements and estimation of raindrop shapes. *J. Atmos. Sci.*, **40**, 1792–1802.
- , 1985: Deducing the microphysical character of precipitation from multiple-parameter radar polarization measurements. *J. Climate Appl. Meteor.*, **24**, 1037–1047.
- , and E. A. Mueller, 1985: Estimation of differential phase shift from sequential orthogonal linear polarization radar measurements. *J. Atmos. Oceanic Technol.*, **2**, 133–137.
- , and J. Davé, 1988: An interpretation of circular polarization measurements affected by propagation differential phase shift. *J. Atmos. Oceanic Technol.*, **5**, 405–415.
- Kostinski, A., 1994: Fluctuations of differential phase and radar measurements of precipitation. *J. Appl. Meteor.*, **33**, 1176–1181.
- Krehbiel, P., 1986: The electrical structure of thunderstorms. *The Earth's Electrical Environment*, E. P. Krider and R. G. Roble, Eds., National Academy Press, 90–113.
- , T. Chen, S. McCrary, W. Rison, G. Gray, and M. Brook, 1996: The use of dual channel circular-polarization radar observations for remotely sensing storm electrification. *Meteor. Atmos. Phys.*, **58**, 65–82.
- McCormick, C., and A. Hendry, 1979: Radar measurement of precipitation-related depolarization in thunderstorms. *IEEE Trans. Geosci. Electron.*, **17**, 142–150.
- McCormick, G. C., 1979: Relationship of differential reflectivity to correlation in dual-polarization radar. *Electron. Lett.*, **15**, 265–266.
- , and A. Hendry, 1975: Principles for the radar determination of the polarization properties of precipitation. *Radio Sci.*, **10**, 421–434.
- , —, and B. L. Barge, 1972: The anisotropy of precipitation media. *Nature*, **238**, 214–216.
- Mead, J. B., P. S. Chang, S. P. Lohmeier, P. M. Langlois, and R. McIntosh, 1993: Polarimetric observations and theory of millimeter-wave backscatter from snow cover. *IEEE Trans. Antennas Propag.*, **41**, 38–46.
- Metcalf, J., 1995: Radar observations of changing orientations of hydrometeors. *J. Appl. Meteor.*, **34**, 757–772.
- , 1997: Temporal and spatial variations of hydrometeor orientations in thunderstorms. *J. Appl. Meteor.*, **36**, 315–321.
- Mott, H., 1986: *Polarization in Antennas and Radar*. John Wiley and Sons, 297 pp.
- Mueller, E. A., 1984: Calculation procedure for differential phase shift. Preprints, *22d Conf. on Radar Meteorology*, Zurich, Switzerland, Amer. Meteor. Soc., 397–399.
- Oguchi, T., 1983: Electromagnetic wave propagation and scattering in rain and other hydrometeors. *Proc. IEEE*, **71**, 1029–1078.
- Rison, W., G. Gray, P. Krehbiel, and T. Chen, 1993: A compact real-time radar signal processing and display system. Preprints, *26th Int. Conf. on Radar Meteorology*, Norman, OK, Amer. Meteor. Soc., 258–259.
- Sachidananda, M., and D. S. Zrnić, 1985: Z_{DR} measurement considerations for a fast scan capability radar. *Radio Sci.*, **20**, 907–922.
- , and —, 1986: Differential propagation phase shift and rainfall rate estimation. *Radio Sci.*, **21**, 235–247.
- Schultz, J., and A. Kostinski, 1997: Variance bounds on the estimation of reflectivity and polarization parameters in radar meteorology. *Geosci. Remote Sens.*, **35**, 248–255.
- Scott, R., 1999: Dual-polarization radar meteorology: A geometrical approach. Ph.D. thesis, New Mexico Institute of Mining and Technology, 129 pp. [Available online at <http://lightning.nmt.edu/radar/scott99/>.]
- Seliga, T., and V. N. Bringi, 1976: Potential use of radar differential reflectivity measurements at orthogonal polarizations for measuring precipitation. *J. Appl. Meteor.*, **15**, 69–76.
- , and —, 1978: Differential reflectivity and differential phase shift: Applications in radar meteorology. *Radio Sci.*, **13**, 271–275.
- Stolzenburg, M., W. D. Rust, B. F. Smull, and T. C. Marshall, 1998a: Electrical structure in thunderstorm convective regions. Part 1: Mesoscale convective systems. *J. Geophys. Res.*, **103**, 14 059–14 078.
- , —, and T. C. Marshall, 1998b: Electrical structure in thunderstorm convective regions. Part 2: Isolated storms. *J. Geophys. Res.*, **103**, 14 079–14 096.
- Tan, J., A. Holt, A. Hendry, and D. Bebbington, 1991: Extracting rainfall rates from X-band CDR radar data by using differential propagation phase shift. *J. Atmos. Oceanic Technol.*, **8**, 790–801.
- Tang, C., and K. Aydin, 1995: Scattering from ice crystals at 94 and 220 GHz millimeter wave frequencies. *Geosci. Remote Sens.*, **33**, 93–99.
- Torlaschi, E., and A. Holt, 1993: Separation of propagation and back-scattering effects in rain for circular polarization diversity S-band radars. *J. Atmos. Oceanic Technol.*, **10**, 465–477.
- , and —, 1998: A comparison of different polarization schemes for the radar sensing of precipitation. *Radio Sci.*, **33**, 1335–1352.
- Zrnić, D., and A. Ryzhkov, 1996: Advantages of rain measurements using specific differential phase. *J. Atmos. Oceanic Technol.*, **13**, 454–464.
- , and —, 1999: Polarimetry for weather surveillance radars. *Bull. Amer. Meteor. Soc.*, **80**, 389–406.